JOURNAL OF CATALYSIS 92, 272–283 (1985)

Chlorine Promotion of Selective Ethylene Oxidation over Ag(110): Kinetics and Mechanism

CHARLES T. CAMPBELL AND BRUCE E. KOEL[1]

Chemistry Division, Los Alamos National Laboratory, Los Alamos, New Mexico 87545

Received September 17, 1984; revised November 6, 1984

The selective oxidation of ethylene to ethylene epoxide ($C_2H_4 + \frac{1}{2} O_2 \rightarrow C_2H_4O$) is catalyzed industrially with a supported Ag catalyst which is promoted for selectivity by adding trace amounts of chlorinated hydrocarbons to the reactant feed. It was recently shown that the role of the chlorine promoters can be modeled by adding chlorine adatoms to a clean Ag(110) surface, and observing how the reaction rates and selectivity vary with chlorine coverage (θ_{Cl}) (C. T. Campbell and M. T. Paffett, *Appl. Surf. Sci.* **19**, 28 (1984); Proceedings, 1983 MRS Symposium, Boston. A continuation of that work is presented in which the reaction kinetics as a function of θ_{Cl} have been carefully mapped. From these data a mechanism for promotion is developed. The experiments are performed in a special apparatus which allows rapid (<20 s) transfer of the model Ag(110) catalyst between an ultrahigh vacuum chamber for surface preparation and analysis (XPS, AES, LEED, TDS) and a high-pressure (<10 atm) microreactor for catalytic rate measurements. It was found that the steady-state reaction rates to produce both ethylene epoxide and $CO_2 + H_2O$ have activation energies and orders in the reactant pressures which vary in characteristic ways with θ_{Cl}. These variations can be very nicely correlated with the electronic effects of θ_{Cl} upon the desorption energies for molecularly adsorbed O_2 and ethylene. These have, however, no relationship to the large increase in selectivity appearing when $\theta_{Cl} > 0.4$ (after nucleation of a $p(2 \times 1)$-Cl structure). It is concluded that the selectivity increase is driven by an ensemble effect, whereby CO_2 production requires more free Ag sites than does epoxide production.

I. INTRODUCTION

The catalytic oxidation of ethylene to ethylene epoxide (also known as ethylene oxide) is of considerable industrial as well as fundamental interest, and has therefore been the subject of intense research activity ((*1–27*) and refs. therein). A typical catalyst is silver supported on α-Al_2O_3 of $\sim 1\ m^2g^{-1}$ specific surface area, which is promoted for selectivity by adding trace amounts of chlorinated hydrocarbons to the reactant feed. The promoter in this case inhibits the conversion of ethylene into the undesirable products $CO_2 + H_2O$, which are strongly thermodynamically preferred. It is estimated that well over $100 million are saved each year in feed costs by chlorine promotion, not to mention the engineering problems this circumvents. Thus, there is a tremendous economic incentive to understand the mechanism of promotion. In addition, a fundamental understanding of this relatively simple system is important for progress toward the goal of chemical tailoring of surface properties.

We have recently studied the kinetics and mechanism of this reaction over clean Ag(110) (*1–4*) and Ag(111) (*5*) single crystal surfaces by using a technique which involves rapid transfer of the catalyst sample between an ultrahigh vacuum (UHV) chamber for surface analyses (AES, LEED, XPS, TDS) and a high-pressure catalytic microreactor for kinetic measurements. We have shown that the dependences of the steady-state reaction rates and selectivity upon temperature and reactant pressures

[1] Address: Cooperative Institute for Research in Environmental Sciences (CIRES) and Chemistry Department, University of Colorado, Boulder, Colorado 80309.

0021-9517/85 $3.00

were virtually identical for clean Ag(110) or Ag(111) and for high-surface area, supported, unpromoted Ag catalysts (*2, 3, 5*). The Ag(110) and (111) surfaces are therefore excellent kinetic models of real-world catalysts. The absolute reaction rates (per surface Ag atom) were some 50- to 100-fold higher on the single crystal surfaces than on the high-surface-area catalysts, a result which is still under discussion (*5*).

We further demonstrated a technique for quantitatively measuring the coverage of atomically adsorbed oxygen (θ_0) existing on the surface under steady-state, high-pressure reaction conditions (*3*). By measuring the reaction rates and selectivity as a function of temperature, reactant pressures, and *also* θ_0, we were able to provide new insights into the controversial reaction mechanism (*3*).

In a preliminary study of the role of chlorine promoters (*1*), we used these techniques to correlate the reaction rates, selectivity, and θ_0 with the coverage of atomically adsorbed chlorine (θ_{Cl}), deposited in a controlled fashion on the Ag(110) surface. These results were also related to the effects of θ_{Cl} upon the adsorption and thermal desorption spectroscopy (TDS) of the reactants, ethylene (Et) and O_2. The conclusions of that study can be summarized as follows. Atomically adsorbed chlorine on Ag(110) has the same effects as chlorinated hydrocarbons in the feed in real catalysis: the selectivity increases to a maximum of about 80% with the loss of considerable activity. Thus chlorinated hydrocarbons simply act to deposit chlorine atoms on the Ag surface, which constitute the true promoter. The support material (e.g., α-Al_2O_3) is not involved. The major effect occurs between the $p(2 \times 1)$ ($\theta_{Cl} = 0.5$) and the $c(4 \times 2)$ ($\theta_{Cl} = 0.75$) chlorine LEED structures, suggesting an ensemble rather than electronic mechanism of promotion. Chlorine rapidly suppresses the rate of dissociative oxygen adsorption, such that θ_0 is negligible for $\theta_{Cl} \geqq 0.3$ under reaction conditions. This has, however, very little effect on the rates or selectivity, indicating that molecularly, not atomically, adsorbed oxygen is the oxidizing agent in the reaction mechanism.

A peroxo form of molecularly adsorbed oxygen ($O_{2,a}$) is well known on Ag(110) (*4, 20–23*). It is thought to lie parallel to the surface, carry a -2 charge, and maintain an O–O bond order of about unity (*4, 20–22*). It has a heat of adsorption of about 10 kcal $mole^{-1}$, and is the precursor to dissociative adsorption (*4, 20–23*). It has been postulated that this species is the actual oxidizing agent in epoxidation ((*7, 10, 11, 18, 19*) and refs. therein), and we support this model (*1, 3*).

The results of our studies support a mechanism (*1, 3*) whereby ethylene, adsorbed through its π orbital, interacts with $O_{2,a}$ in the formation of an intermediate complex. This intermediate can then either evolve ethylene epoxide (EtO), leaving an oxygen adatom behind on the surface, or dissociate, leading to $CO_2 + H_2O$ production. The intermediate formation is rate limiting under many conditions. After epoxide formation, the remaining oxygen adatom must in all cases go to either CO_2 or H_2O product. According to this model, this sets an upper limit on the selectivity of 6/7 (in terms of ethylene conversion to EtO), which is identical to the observations for optimally promoted catalysts (*1, 12, 24*). However, these also appears to exist a second minor path to $CO_2 + H_2O$ production (*3*) whereby ethylene dissociation to some fragments occurs, followed by oxidation of the fragments by O_a. The adsorbed ethylene reactant is stabilized with respect to desorption by both O_a and Cl_a, which withdraw electron density from the Ag, facilitating π-electron donation ((*1*) and refs. therein). We note that the above mechanism is supported by other detailed kinetic studies on high-area Ag catalysts ((*10, 11, 14, 19, 26*) and especially (*18*)), and that very similar mechanisms have been previously proposed (*18, 26*).

The objective of the present study is to

extend our kinetic information on the effects of θ_{Cl} upon the steady-state reaction rates and selectivity to a wide range of temperature and pressure conditions. The goal here is to map out the reaction orders (in P_{Et} and P_{O_2}) and activation energies for both EtO and CO_2 ($+H_2O$) production, and to determine how these vary with promoter concentration (θ_{Cl}). It was hoped that we could correlate changes in the reaction orders and activation energies with increases in the selectivity. Instead, it is found that the changes with θ_{Cl} in activation energy and reaction orders for CO_2 production always paralleled those for EtO production, such that correlation of these parameters with the increase in selectivity seems impossible. This further supports our previous contention (*1*) that the selectivity increase is related to an ensemble, or site, requirement. It *is* found, however, that the variations in reaction orders and activation energies correlate very strongly with the electronic effects of chlorine addition upon the heats of adsorption of $O_{2,a}$ and $C_2H_{4,a}$, consistent with our reaction mechanism.

II. EXPERIMENTAL

The Ag(110) preparation technique is described in another paper (*4*). Details of the apparatus and technique are presented in a related paper (*3*). In short, the Ag(110) sample was cleaned by sputtering and annealing (800 K) in ultrahigh vacuum (UHV), and its cleanliness and order were proven by Auger electron spectroscopy (AES), X-ray photoelectron spectroscopy (XPS), and low-energy electron diffraction (LEED). The clean surface was then dosed with chlorine adatoms by one of two methods which we described previously (*1*). The chlorine coverage was then determined by AES. The Cl(LMM)/Ag(MNN) peak-to-peak ratio (I_{Cl}/I_{Ag}) was taken as proportional to θ_{Cl}, and calibrated against a coverage $\theta_{Cl} = 0.75$, which gives a distinct $c(4 \times 2)$-Cl LEED pattern ((*1*) and refs. therein). The sample, thus prepared and characterized, was transferred into an evacuated microreactor attached directly to the UHV chamber, pressurized with the reaction mixture (~100 Torr) and heated (440–610 K) until a steady-state epoxidation rate (2–4 min) was established. A constant rate of EtO production was actually established in <20 s, and could be maintained over time periods during which >5000 molecules of ethylene per surface Ag atom were converted to products. Conversions were typically about 3% (see (*3*)). Then the sample was rapidly (17 s) transferred at reaction temperature back into UHV for surface analysis (AES, LEED, TDS, XPS). The coverage of O_a was quantitatively measured by flash heating the sample immediately after transfer and measuring the area under the 600 K O_2 thermal desorption peak mass-spectrometrically (*3*). The chlorine coverage was reconfirmed by AES after reaction, to ensure that it did not change significantly. After transfer, the reaction mixture (still in the batch microreactor) was analyzed by gas chromatography for the amount (rates) of EtO and CO_2 produced. As discussed in related papers (*1, 3*), above 480 K the surface contained only atomically adsorbed oxygen (O_a) and chlorine (Cl_a) and maintained a good LEED pattern after reaction. Below 480 K other adsorbed reactants and products were observed. The sides and back of the crystal were passivated to reaction by a mixed Si, Cu, Ti oxide/carbide film which built up during the early stages of high-pressure reaction attempts (*3*).

We point out that while the chlorine coverage did not change during the time (2–4 min) required to establish steady-state reaction rates, the reaction mixture is known to remove chlorine slowly from the surface. This is why chlorine must be added continuously at low levels (ppm) to the reactant feed in industrial processes. Obviously, this removal process is slow on the time scale used here.

Coverages (θ) are defined relative to the number of Ag surface atoms ($\theta = 1$ is 8.5×10^{14} cm^{-2}). Specific rates were calculated

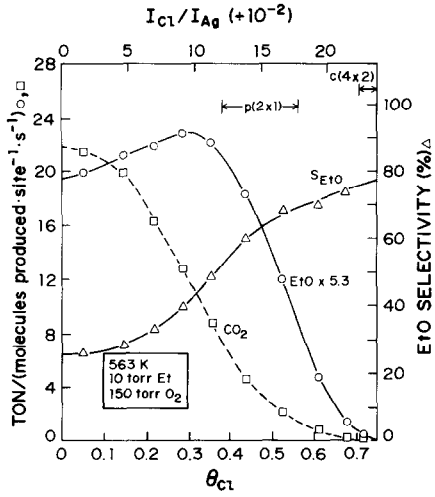

FIG. 1. Steady-state reaction rates and selectivity versus chlorine coverage at 563 K, 10 Torr Et, and 150 Torr O_2.

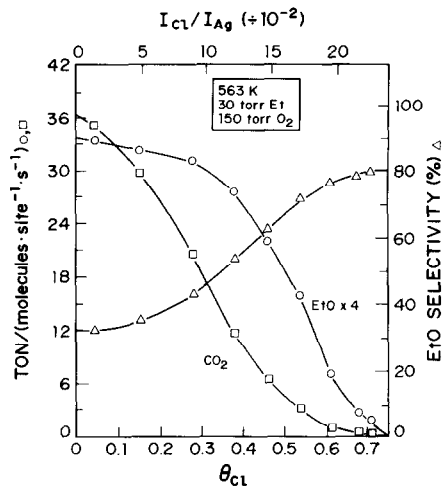

FIG. 3. Steady-state reaction rates and selectivity versus chlorine coverage at 563 K, 30 Torr Et, and 150 Torr O_2.

assuming 10^{15} Ag surface atoms, although the geometric surface area would dictate using a value of 4.6×10^{14}.

Due to a failure of the electron gun, in some cases the Cl(2*p*)/Ag(3*d*) XPS intensity ratio was used to measure θ_{Cl}. Calibration was the same as for the AES ratio above. The Cl(2*p*) peak appeared as a spin–orbit split doublet at 197.7 and 199.0 eV B.E. (binding energy), referenced as in (*4*) to the Fermi level.

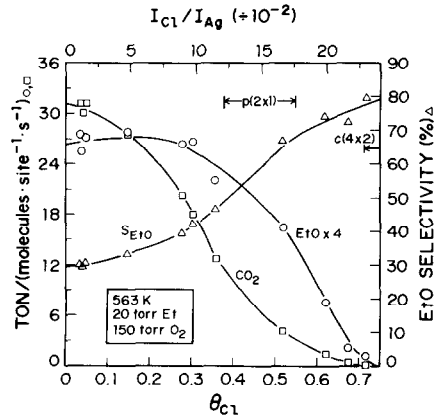

FIG. 2. Steady-state reaction rates and selectivity versus chlorine coverage at 563 K, 20 Torr Et, and 150 Torr O_2.

III. RESULTS

III.1. Kinetics

The variation in the steady-state rates of EtO and CO_2 production and the selectivity with θ_{Cl} are shown for 563 K, $P_{O_2} = 150$ Torr, and $P_{Et} = 10$, 20, and 30 Torr in Figs. 1–3, respectively. The rates are expressed as turnover numbers (TON), i.e., the number of molecules of that product produced per second per surface silver atom. The selectivity is defined with respect to ethylene conversion: $S_{EtO} = TON_{EtO}/(TON_{EtO} + \frac{1}{2} TON_{CO_2})$. Also shown in Figs. 1 and 2 are the coverage regions over which $p(2 \times 1)$-Cl and $c(4 \times 2)$-Cl LEED patterns are observed after reaction (*1*). The ideal coverages for these structures are considered to be 0.5 and 0.75, respectively ((*1*) and refs. therein).

From Figs. 1–3, it is straightforward to extract the reaction orders in ethylene pressure (*n*) at 563 K, 20 Torr Et and 150 Torr O_2 and any given chlorine coverage. This result is presented in the top section of Fig. 4. For both EtO and CO_2 production, *n* decreases with θ_{Cl} until $\theta_{Cl} \simeq 0.3$, after which it increases to a value above that of the clean surface.

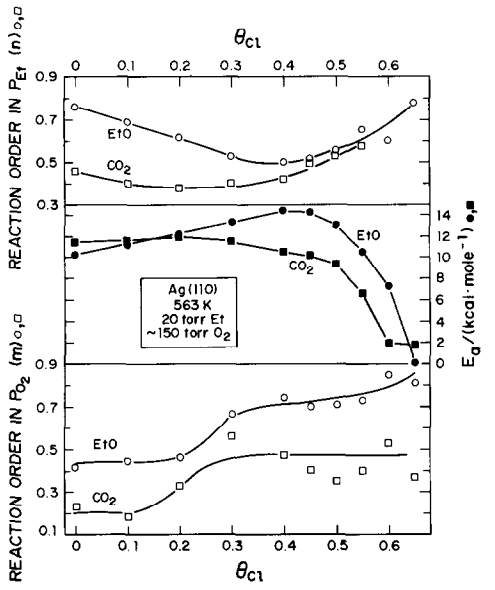

FIG. 4. Steady-state reaction orders in P_{O_2} and P_{Et} and activation energies (E_a) versus chlorine coverage near 563 K, P_{Et} = 20 Torr, and P_{O_2} = 150 Torr. Exact condition ranges are: for n, P_{O_2} = 150 Torr, T = 563 K, P_{Et} = 10–30 Torr (Figs. 1–3); for E_a, P_{O_2} = 150 Torr, P_{O_2} = 20 Torr, T = 540–590 K; and for m, P_{Et} = 20 Torr, T = 563 K, P_{O_2} = 50–150 Torr.

Data similar to that in Figs. 1–3 was repeated over a range of pressures and temperatures. Expressing the reaction rates as

$$\text{TON} = \nu \exp(-E_a/RT)P_{Et}^{n}P_{O_2}^{m}, \quad (1)$$

we were able to determine the activation energies (E_a) and reaction orders in $P_{Et}(n)$ and $P_{O_2}(m)$ for both EtO and CO_2 production as a function of θ_{Cl}. This was achieved by holding two values constant and varying the other (T, P_{Et}, or P_{O_2}) and θ_{Cl}. An example of this type of analysis, in this case an Arrhenius plot to determine the activation energy for CO_2 production, is shown in Fig. 5. One can see that at low temperatures E_{a,CO_2} is fairly insensitive to θ_{Cl}, but at 563 K it decreases rapidly when θ_{Cl} exceeds 0.5. Least-squares fits were performed on the data in the appropriate linear functional forms to determine E_a, n, and m quantitatively.

The results for 563 K, 20 Torr Et, and ~150 Torr O_2 are compiled in Fig. 4. These can of course be directly compared with the rates and selectivity at these conditions in Fig. 2. The condition ranges over which the parameters in Fig. 4 were determined are listed in the caption. Evaluation at $\theta_{Cl} > 0.65$ was impossible due to the small value of the rates and their strong dependence upon θ_{Cl}. The activation energy for EtO slowly increases until $\theta_{Cl} \gtrsim 0.4$, after which it decreases rapidly, ending up near zero. A similar result is seen for CO_2, although the initial increase in E_a is weaker and stops already when $\theta_{Cl} \gtrsim 0.2$. The reaction orders in O_2 pressure, m, start out low, go through a marked increase for $0.1 < \theta_{Cl} < 0.3$, above which they stabilize or slightly increase.

To demonstrate that similar trends are seen at other conditions, we show in Fig. 6 the values of m and E_a versus θ_{Cl} at 490 K, 4.1 Torr Et, and 16 Torr O_2. The variation in the rates and selectivity with θ_{Cl} at conditions quite close to these have been presented in our previous paper (*1*), and so will not be reproduced here. By comparing Figs. 4 and 6, it appears that the increase in m with θ_{Cl} occurs at higher θ_{Cl} when m on

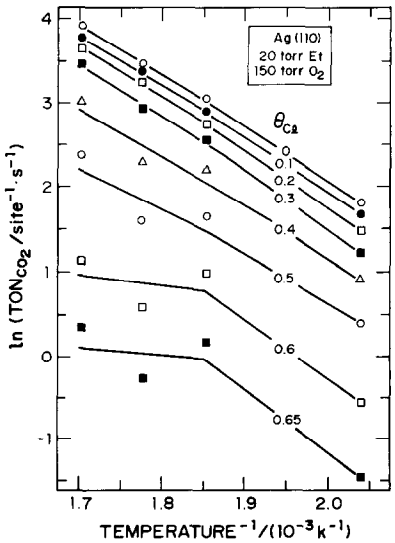

FIG. 5. Arrhenius plots at various chlorine coverages of the steady-state rate of CO_2 production versus temperature at 20 Torr Et and 150 Torr O_2.

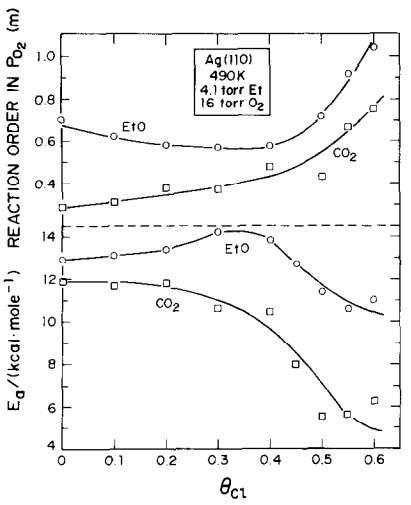

FIG. 6. Steady-state reaction orders in P_{O_2} and activation energies (E_a) versus chlorine coverage near 490 K, 4.1 Torr Et, and 16 Torr O_2. Exact conditions are: for m, T = 490 K, P_{Et} = 4.1 Torr, P_{O_2} = 8–32 Torr; and for E_a P_{Et} = 4.1 Torr, P_{O_2} = 16 Torr, T = 490–540 K.

the clean surface is higher. We will not discuss Fig. 6 in detail. Its purpose is simply to demonstrate that the changes seen in Fig. 4 are qualitatively reproduced at other temperature and pressure conditions. However, the chlorine coverages at which the kinetic parameters change may depend upon the exact conditions of pressure or temperature. This also applies to the extent of these changes.

III.2. Thermal Desorption

In our previous work (*1*), we demonstrated the effects of θ_{Cl} upon the thermal desorption behavior of ethylene and the dissociative sticking probability of O_2 on Ag(110). Chlorine increased the saturation coverage and heat of adsorption of molecularly adsorbed ethylene, from 8.9 kcal mole^{-1} for the clean surface to 12.8 kcal mole^{-1} for $\theta_{Cl} \cong 0.4$. Above θ_{Cl} = 0.5, the heat of adsorption again decreases with increasing θ_{Cl}. The dissociative sticking probability for O_2 at 477 K decreases rapidly with increasing θ_{Cl} and is essentially zero by θ_{Cl} = 0.3.

Figure 7 shows the effect of chlorine upon molecular and dissociative O_2 adsorption, using thermal desorption spectroscopy. We gave a 2400 L (L = Langmuir = 10^{-6} Torr · s) O_2 dose at 130 K to surfaces with various precoverages of Cl_a. The results on the clean surface are well known ((*4*) and refs. therein). At 130 K, O_2 is almost entirely molecularly adsorbed on the clean surface as the peroxo-like species. Upon heating, this species partially desorbs as O_2 at ~185 K (10 kcal mole^{-1}) and partially dissociates, depositing O_a on the surface. The oxygen adatoms later associatively desorb at ~605 K. As seen in Fig. 7, the dissociative peak (605 K) is rapidly suppressed with increasing chlorine coverage, becoming negligible by θ_{Cl} = 0.26. This simply reflects previous measurements of the effects of θ_{Cl} upon the dissociative sticking probability for O_2 (*1, 11, 13, 14*). The molecular state (185 K) is almost unaffected until θ_{Cl} exceeds 0.25, above which the peak shifts slowly to lower temperature and decreases in intensity, reflecting a decrease in the heat of adsorption of $O_{2,a}$.

The O(1*s*)-XPS binding energy for $O_{2,a}$ in the presence of θ_{Cl} = 0.15 was measured by a method identical to that described in (*4*) for $O_{2,a}$ on the clean surface, but with

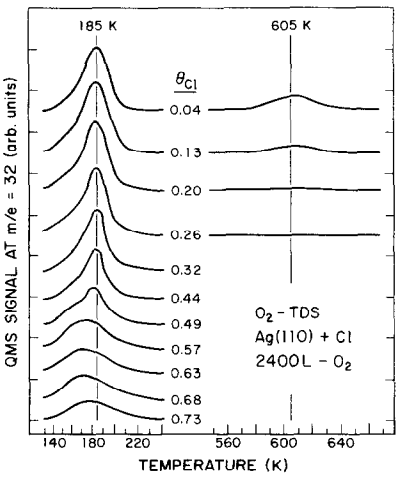

FIG. 7. Thermal desorption spectra of O_2 following a 2400-L O_2 dose at 130 K to the clean Ag(110) surface with varying precoverages of chlorine as shown. (β = 14 K · s^{-1} near 185 K and 11 K · s^{-1} near 600 K.)

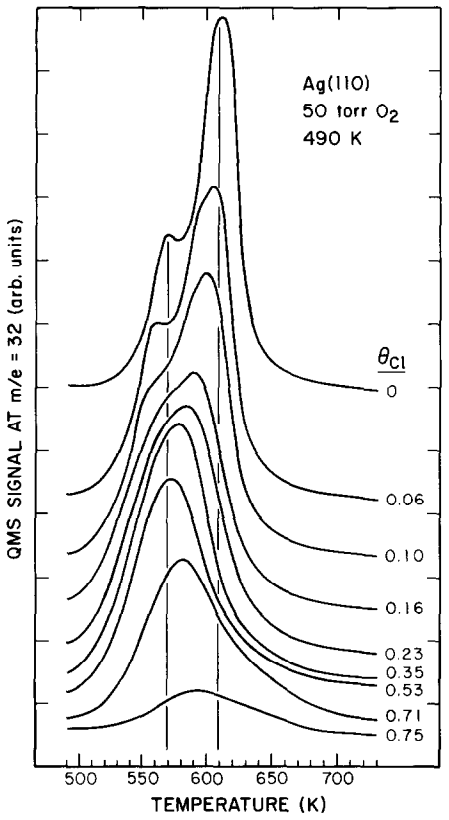

FIG. 8. Thermal desorption spectra of O_2 following a 20-s, 50-Torr O_2 dose at 490 K to the clean Ag(110) surface containing various precoverages of chlorine as shown. The sample was transferred at 490 K from the microreactor into UHV ($<2 \times 10^{-8}$ Torr) and TDS was begun in less than 20 s after completion of the dose (*4*) ($\beta = 12$ K · s^{-1}).

poorer statistics. No large difference is seen between $O_{2,a}$ on the clean surface and on a surface with $\theta_{Cl} = 0.15$, except that the O(1*s*) peak is shifted about 0.1 eV to higher binding energy and perhaps broadened.

To see if O_2 could dissociatively adsorb to any extent for chlorine coverages above 0.3, we exposed the surface with various chlorine precoverages to an excessive O_2 dose (50 Torr for 20 s) at 490 K. This exposure on the clean surface gives a pure adlayer of atomic oxygen with a sharp $c(6 \times 2)$-O LEED pattern, corresponding to $\theta_0 = 0.67$ (*4*). This structure desorbs in two peaks (~570 and 610 K) which have been described in detail (*4*). The $c(6 \times 2)$-O pattern reverts to the well-known $p(2 \times 1)$-O (i.e., $\theta_0 = 0.5$) upon desorption of the lower temperature peak (*4*). The desorption results are shown in Fig. 8. With increasing chlorine coverage, both peaks shift to lower temperature and are suppressed at the expense of a single, broad peak at about 580 K. The oxygen coverage (area under the peaks) is almost constant until $\theta_{Cl} > 0.25$, then decreases only slightly (~33%) with θ_{Cl} until $\theta_{Cl} > 0.70$, after which it suddenly decays for saturation coverage of chlorine ($\theta_{Cl} = 0.75$). While LEED showed the expected patterns for the chlorine precoverages, these patterns were obliterated and showed a very high background intensity after the oxygen dose for $0.45 < \theta_{Cl} < 0.70$. (LEED observations were not made at other chlorine coverages, except $\theta_{Cl} \leqq 0.06$, where the O_2 dose generated a sharp $c(6 \times 2)$-O pattern, as mentioned above for the clean surface). The severe disorder in LEED would suggest that perhaps the oxygen or chlorine moves beneath the surface Ag layer, destroying the long-range order in the topmost Ag layers. Subsurface oxygen desorbs at about these same temperatures from Ag(110) ((*4*) and refs. therein).

We note that the results in Fig. 8 differ somewhat from a previous report (*15*), which showed that the "saturation" oxygen coverage on Ag(110) decayed linearly with θ_{Cl}, becoming negligible by $\theta_{Cl} = 0.5$. This difference is likely due to the smaller exposure or temperature used in (*15*).

IV. DISCUSSION

Our results will be discussed on the basis of the mechanism presented in the Introduction. By this mechanism, adsorbed ethylene and molecularly adsorbed (peroxo-) O_2 combine in the formation of an intermediate, I_a. This intermediate can then branch out to yield epoxide + O_a or the decomposition products, $CO_2 + H_2O$. Formation of I_a is rate limiting in both EtO and CO_2 production under many conditions. A second parallel pathway to CO_2, involving ethylene dissociation and O_a, is only of minor impor-

tance here. Similar mechanisms have been proposed previously (*18, 26*).

According to this model, the reaction orders in P_{O_2} and P_{Et} will be determined by the extent to which the coverages of molecularly adsorbed O_2 and Et track P_{O_2} and P_{Et}, respectively. At saturation coverage, θ will not vary with pressure; and, the order will be zero. At low θ, the order will be high. The effects of chlorine coverage upon the reaction orders in P_{O_2} and P_{ET} (Figs. 4 and 6) correlate very well with the effects of chlorine upon the heats of adsorption of $O_{2,a}$ and Et_a as measured by TDS (Fig. 7 and Ref. (*1*)). Chlorine decreases the heat of adsorption of $O_{2,a}$ (Fig. 7). This should decrease the steady-state coverage of this species under reaction conditions and eventually lead to an increase in the reaction order in $P_{O_2}(m)$, provided $O_{2,a}$ is involved in the rate-determining step. This is in fact observed (Figs. 4 and 6). Chlorine increases the heat of adsorption of ethylene in the range $0 < \theta_{Cl} < 0.35$ (*1*). Conversely, this should increase the steady-state coverage of Et_a and decrease the reaction orders (n) in P_{Et}, provided, Et_a is involved in the rate-determining step. Again, this matches the observation (Fig. 4). These results are consistent with the proposed mechanism.

If the order in P_{Et} is high enough, this latter effect will even lead to an increase in the rate with θ_{Cl}. This feature was indeed observed in the EtO production rate at low P_{Et}/P_{O_2} ratios (see Fig. 1, for example), where n exceeds unity on the clean surface. (The reaction order in P_{Et} for EtO production, n_{EtO}, approaches two on the clean surface as P_{Et}/P_{O_2} approaches zero (*3*).) In these cases, chlorine can be considered a true activity promoter, as well as selectivity promoter. While chlorine is generally considered to decrease the activity of industrial Ag catalysts (*6–13*), an increase in both activity and selectivity at low chlorine levels has been observed in at least one case (*25*).

When θ_{Cl} exceeds 0.5 (beyond completion of the $p(2 \times 1)$-Cl structure), chlorine addition strongly decreases the heat of adsorption of ethylene (*1*). Here, the steady-state coverage of Et_a should decrease and the reaction orders (n) in P_{Et} should increase. This is indeed observed (Fig. 4). The minimum in n versus θ_{Cl} ($\theta_{Cl} \cong 0.4$, Fig. 4) corresponds very closely to the maximum in the desorption peak temperature for Et versus θ_{Cl} ($\theta_{Cl} \cong 0.4$ (*1*)). The changes in the reaction orders with θ_{Cl} correspond surprisingly well to the changes in the heats of adsorption with θ_{Cl}.

Note that the orders in both P_{Et} and P_{O_2} are approaching unity as chlorine approaches the saturation $c(4 \times 2)$ level (Figs. 4, 6). In this case, the reaction is limited by the supply of reactants, $O_{2,a}$ and Et_a, to the surface. That is, the adsorption steps are rate determining. The severe blocking of the surface by adsorbed chlorine must drive the reaction to this situation of reactant-supply limitation. We note that the structure which has been proposed for the $c(4 \times 2)$-Cl structure closely resembles the (111) surface of the layered compound AgCl, with a nearly hexagonal array of chlorine as the topmost layer (*16*). In this structure, it is sterically impossible for an ethylene molecule to approach the underlying Ag surface closely enough for its π orbitals to overlap sufficiently with a Ag atom for dative bond formation. It is thus not difficult to understand why the rates go to zero on this structure.

At slightly lower coverages, vacancies will open up for adsorption. Let us assume that two vacancies, side by side, are required for simultaneous adsorption of Et and O_2 in a configuration suitable for reaction. Under static conditions, the concentration of such "double vacancies" and therefore the rates would simply scale as $(0.75 - \theta_{Cl})^2$. The reaction orders in P_{O_2} and P_{Et} would not necessarily approach unity. Under dynamic conditions, however, chlorine will move about on the surface and such "double-vacancies" will be continuously created and destroyed. It is now required that both an O_2 molecule and an ethylene molecule reach the "double

vacancy" before it is destroyed. If the site destruction rate (by Cl hopping) exceeds the reactant impingement frequency ($\sim 10^6$ s^{-1}) the reaction will necessarily be limited by the supply of reactants.

Under these conditions, the selectivity always seems to approach a maximum value of about 80% quite close to the theoretical limit (see Introduction) of 6/7. According to the proposed mechanism, this arises because all branching pathways to CO_2 are suppressed. Now CO_2 can only be produced from an oxygen adatom (O_a) which is created as a by-product of the process: $Et_a + O_{2,a} \rightarrow I_a \rightarrow EtO + O_a$, where I_a is the intermediate. This intermediate normally could decompose to CO_2 and water. It is not difficult to envision how this decomposition branch is suppressed rapidly with θ_{Cl} according to a site size, or ensemble, requirement. Decomposition, almost by definition, requires several sites to accommodate the products. The exact nature of this decomposition process and its ensemble requirement would be purely speculative at this point, although strong inverse kinetic isotope effects suggest that C–H bond cleavage initiates the process (*26*). The intermediate, I_a, may be related to a species seen in the presence of Et + O_2 on silver catalysts which shows an O–O stretch frequency of 870 cm^{-1} (*14*) or to other suggested species (*18, 26, 27*). Note that $O_{2,a}$ has a stretch frequency of 640 cm^{-1} (*20–22*) on Ag(110).

Returning to Fig. 4, changes with θ_{Cl} in the activation energies closely reflect changes in the reaction orders in P_{Et} (n). The increase in E_a as n decreases for $0 < \theta_{Cl} < 0.4$ can be readily understood on the basis of a model we used previously to explain the decrease in E_a with temperature on the clean surface (*3*). According to that argument, the true activation energy (E_a^{true}) for the rate-limiting elementary step ($Et_a + O_{2,a} \rightarrow I_a$) is around 22 kcal $mole^{-1}$. The reaction rates can then be written as

$$TON = \nu' \exp(-E_a^{true}/RT)\theta_{Et}\theta_{O_2}, \quad (2)$$

where the branching ratio of the intermediate will determine ν' for EtO or CO_2. The apparent activation energy will depend upon E_a^{true} and the variation in θ_{Et} and θ_{O_2} with temperature. It will decrease by an amount equal to the heat of adsorption (ΔH_{ad}) of one or both of these reactants when the coverage of that species is low and determined by adsorption/desorption equilibrium. This is generally the case when the reaction order in that species (i) is high. Under these conditions we can write

$$\theta_i \propto P_i \exp[\Delta H_{ad,i}/RT]. \quad (3)$$

For Fig. 4, ethylene is approaching these conditions on clean surface. The observed activation energy for EtO production (~ 10 kcal $mole^{-1}$, Fig. 4) is thus close to the true activation energy of 22 kcal $mole^{-1}$ minus the heat of Et adsorption (~ 10 kcal $mole^{-1}$ (*1*)). But as θ_{Cl} increases, the reaction order in P_{Et} decreases strongly, indicating that the coverage of Et_a is no longer so low that Eq. (3) is valid. The coverage now varies less strongly with temperature, and the apparent activation energy increases back towards its true value. When $\theta_{Cl} \gtrsim 0.4$, the reaction orders in P_{Et} reverse the trend and start to increase. Accordingly, the activation energies start to decrease. Finally, when $\theta_{Cl} \simeq 0.65$, the reaction orders in both P_{Et} and P_{O_2} are approaching unity, so that Eq. (3) is valid for both Et and O_2 adsorption. The apparent activation energies are then close to zero, in agreement with Eqs. (2) and (3), whereby the true activation energy (~ 22 kcal $mole^{-1}$) is decreased by both $\Delta H_{ad,Et}$ (~ 10 kcal $mole^{-1}$) and $\Delta H_{ad,O_2}$ (~ 10 kcal $mole^{-1}$ (*4*)).

In observing Figs. 4 and 6, one feature is overwhelmingly obvious. The variations in E_a, m, and n for CO_2 production with θ_{Cl} almost completely parallel the variations for EtO production. Very strong kinetic similarities in EtO and CO_2 production rates have been pointed out previously (*3, 7, 19, 26, 27*), and are a major argument in favor of a common rate-determining *slow* step leading to an intermediate, which can

then *rapidly* branch out to either CO_2 + H_2O or EtO production. Note that according to this model, a change in the rates of these rapid branching steps due to θ_{Cl} will not be manifested as changes in E_a, m, or n (since the branching is not the rate-determining step). It may readily manifest itself as a change in the selectivity (provided the two branches are affected differently by θ_{Cl}). This is precisely what we believe is occurring here. Thus, we see no changes with θ_{Cl} in E_a, m, or n for EtO as compared to CO_2 production (Fig. 4) which can be correlated with the marked selectivity changes of Fig. 2. The changes in E_a, m, and n do, however, correlate strongly with the effects of θ_{Cl} upon the heats of adsorption of $O_{2,a}$ and Et_a, as pointed out above. This is further support of the participation of these species in the rate-determining step: $Et_a + O_{2,a} \rightarrow I_a$.

Consider the branching steps, whereby the intermediate I_a decomposes into either EtO + O_a or into species which ultimately produce CO_2 + H_2O. It is quite reasonable to assume that these two reaction pathways have strongly different site requirements. In the former case, no bonds need to be completely broken in the ethylene molecule, and at most only two decomposition products need to be accommodated to sites on the surface. On the other hand, for CO_2 + H_2O production, all five bonds in the ethylene molecule must ultimately be broken and many fragments must somehow be stabilized at the surface. As a first guess, one would certainly expect that the latter path requires a larger ensemble of free Ag atoms. We feel that it is this ensemble requirement which causes the rate of CO_2 production to decay so much more rapidly with θ_{Cl} than that of EtO production in Figs. 1–3. This, in turn, results in the selectivity increase with θ_{Cl}.

We now turn to a discussion of the effects of chlorine on the interaction of oxygen with the Ag(110) surface. Combining our results with previous work (*1, 4, 20–23*), it is now possible to construct a potential energy diagram which qualitatively indicates the effects of added chlorine (Fig. 9). A strong decrease in the dissociative sticking probability for O_2 with θ_{Cl} in the coverage range $0 < \theta_{Cl} < 0.25$ has been reported previously (*1, 13, 14*) and is reflected in the decrease in the high-temperature peak area in Fig. 7. This effect can be understood in terms of the simple two-dimensional potential energy model shown in Fig. 9. In this coverage range, $\Delta H_{a,O_2}$ is not much affected by the presence of chlorine (see Fig. 7). However, $\Delta H_{a,O}$ decreases noticeably with θ_{Cl}, as can be seen in Fig. 8 or Ref. (*15*). This will lead to a higher curve crossing for the molecular versus dissociative states, as shown by the dashed curve in Fig. 9. Thus the activation energy for dissociation, E_a^{diss}, increases upon chlorine addition. The dissociative sticking probability will be determined by a competition in pathways for $O_{2,a}$. It can either desorb again as O_2, or climb the barrier E_a^{diss} and form two chemisorbed atoms. Here E_a^{diss} is increasing

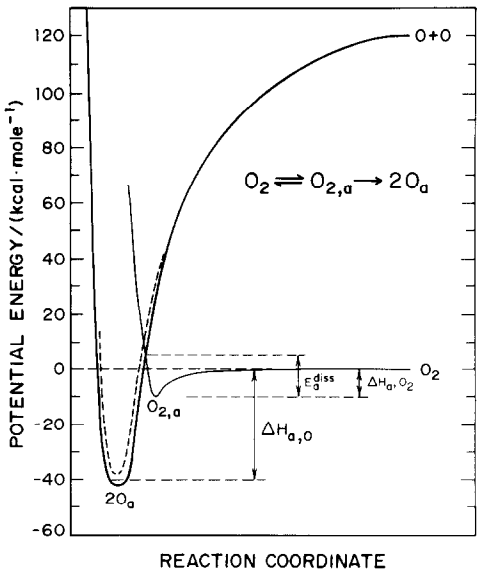

FIG. 9. Model potential energy surface for O_2 and O interacting with a clean Ag(110) surface, showing the relationship of the heats of adsorption to the dissociation energy and probability. The dashed curve represents the change expected upon chlorine addition for $\theta_{Cl} \leqq 0.25$.

with θ_{Cl} without $\Delta H_{a,O_2}$ being strongly effected, so the dissociation process will become less likely. This decrease in the dissociative sticking probability fed directly into the steady-state coverage of O_a under reaction conditions, as indicated previously (*1*). In the present work we have not attempted to measure θ_0, as our temperature here was too high for such measurements in general, and because O_a appears to play no direct role in the rate-limiting step (*1, 3, 5*).

The study of molecular O_2 adsorption as performed in Fig. 7 was very difficult in our apparatus for two reasons: (1) the required O_2 dose at our minimum temperature (~130 K) was very large (2400 L), and (2) the sample region had been exposed to high pressures (up to 600 Torr) of the reaction/product mixture and therefore was somewhat "dirty." For this reason the O_2 adlayers formed were often coadsorbed with about 10% impurities (mostly H_2O, CO_2, and CO). We were unable to improve upon this situation, and so have used these data, which we believe are at least qualitative indication of the effects of chlorine upon molecular O_2 adsorption. We would be glad to see these experiments repeated in a more standard UHV apparatus, particularly with some additional spectroscopy such as HREELS to confirm the effects of Cl_a upon $O_{2,a}$.

V. CONCLUSIONS

The type of data presented in Figs. 4 and 6 represent a new dimension to which surface science techniques can be applied to understanding the role of chemical modifiers in catalysis. We have shown that it is now possible to map out the rates, reaction orders, and activation energies in detail as a function of the surface coverage of the modifier on well-defined surfaces. These experiments are relatively easy and rapid, and provide unique insight into the mechanism of modification. Such experiments would be prohibitively time consuming and lack the necessary degree of control, if approached with the methodology of classical catalysis.

VI. ACKNOWLEDGMENT

One of us (C.T.C.) acknowledges partial support of this work by the DOE Office of Basic Energy Sciences, Materials Science Division.

REFERENCES

1. Campbell, C. T., and Paffett, M. T., *Appl. Surf. Sci.* **19,** 28 (1984); Proceedings, 1983 MRS Symposium, Boston.
2. Campbell, C. T., *J. Vac. Sci. Technol. A2* (1984) 1024.
3. Campbell, C. T., and Paffett, M. T., *Surf. Sci.* **139,** 396 (1984).
4. Campbell, C. T., and Paffett, M. T., *Surf. Sci.* **143,** 517 (1984).
5a. Campbell, C. T., submitted to *J. Catal.*
5b. Campbell, C. T., submitted to *Surf. Sci.*
6. Kummer, J. T., *J. Phys. Chem.* **60,** 666 (1956).
7. Voge, H. H., and Adams, C. R., "Advances in Catalysis," Vol. 17, p. 151. Academic Press, New York, 1967.
8. Ostrovskii, V. E., Kul'kova, N. V., Lopatin, V. L., and Temkin, M. I., *Kinet. Katal.* **3,** 160 (1962).
9. Margolis, L. Y., Enikeev, E. K., Isaev, O. V., Krylova, A. V., and Kuchnerov, M. Y., *Kinet. Katal.* **3,** 153 (1962).
10. Verykios, X. E., Stein, F. P., and Coughlin, R. W., *Catal. Rev.-Sci. Eng.* **22,** 197 (1980).
11. Kilty, P. A., and Sachtler, W. M. H., *Catal. Rev.-Sci. Eng.* **10,** 1 (1974).
12. Giordano, N., Bart, J. C. J., and Maggiore, R., *Z. Phys. Chem. NF* **127,** 109 (1981).
13. Meisenheimer, R. G., and Wilson, J. N., *J. Catal.* **1,** 151 (1962).
14. Kilty, P. A., Rol, N. C., and Sachtler, W. M. H., "Proceedings, 5th International Congress on Catalysis, Palm Beach, 1972" (J. W. Hightower, Ed.), Vol. 2, p. 929. North-Holland, Amsterdam, 1973.
15. Rovida, G., Pratesi, F., and Ferroni, E., *J. Catal.* **41,** 140 (1976).
16. Rovida, G., and Pratesi, F., *Surf. Sci.* **51,** 270 (1975).
17. Marbrow, R. A., and Lambert, R. M., *Surf. Sci.* **71,** 107 (1978).
18. Van Santen, R. A., Moolhuysen, J., and Sachtler, W. M. H., *J. Catal.* **65,** 478 (1980).
19. Sachtler, W. M. H., Backx, C., and van Santen, R. A., *Catal. Rev. Sci. Eng.* **23,** 127 (1981).
20. Backx, C., de Groot, C. P. M., and Biloen, P., *Appl. Surf. Sci.* **6,** 256 (1980).
21. Sexton, B. A., and Madix, R. J., *Chem. Phys. Lett.* **76,** 294 (1980).
22. Backx, C., de Groot, C. P. M., and Biloen, P., *Surf. Sci.* **104,** 300 (1981).

23. Barteau, M. A., and Madix, R. J., "The Chemical Physics of Solid Surfaces and Heterogeneous Catalysis" (D. A. King and D. P. Woodruff, Eds.), Vol. 4, Chap. 4. Elsevier, Amsterdam, 1982.
24. Zomerdijk, J. C., and Hall, M. W., *Catal. Rev.-Sci. Eng.* **23,** 163 (1981).
25. Montrasi, G. L., and Battison, G. C., *Oxid. Commun.* **3,** 259 (1983).
26. Cant, N. W., and Hall, W. K., *J. Catal.* **52,** 81 (1978).
27. Force, E. L., and Bell, A. T., *J. Catal.* **40,** 356 (1975).